Supplementary information

Rapid preparation of Imide-based COF Films through Electropolymerization Integrated with Low-temperature Annealing for High-performance Electrochromic Energy Storage

Jinming Zeng*[a], Huiling Hou[a], Lei Huang[a], Zheng Xie[a], Qingqing Qiu[a], Huan Li[a], Dongfa Liu[a, c], Putrakumar Balla[d], Tongxiang Liang[a], Ping Liu*[b]

[a] *Jiangxi Provincial Key Laboratory of Magnetic Metallic Materials and Devices & College of Rare Earths, Jiangxi University of Science and Technology, Ganzhou 341000, PR China*
[b] *State Key Laboratory of Luminescent Materials and Devices, South China University of Technology, Guangzhou 510640, PR China*
[c] *Nankang No.6 High School, Ganzhou, Jiangxi 341400, PR China*
[d] *Department of Chemical Engineering and Applied Chemistry, Chungnam National University, Daejeon, 34134, South Korea*

Table of Contents

Experimental section

S1 Materials

N,N,N',N'-tetrakis(4-aminophenyl)-1,4-phenylenediamine (TPPDA), 9,9-Bis(3,4-dicarboxyphenyl)fluorene dianhydride (DFD), and Tetrabutylammonium perchlorate (TBAP) were purchased from Shanghai Aladdin Biochemical Technology Co., Ltd. 1,4,5,8-naphthalenetetracarboxylic dianhydride (NTCDA) was purchased from Shanghai Bide Pharmaceutical Technology Co., Ltd. Dichloromethane was purchased from Xilong Chemical Co., Ltd. Propylene carbonate was purchased from Shanghai Macklin Biochemical Technology Co. Ltd.. All commercial reagents were used as received without further purification. ITO glasses (14 Ω/sq, Zhuhai Kaivo) were cut into 0.9×4.0 cm^2 and washed using acetone, deionized water, and ethanol in an ultrasonic environment for 15 min, and then dried to obtain clean ITO glasses.

S2 Characterization

Fourier-transform infrared (FT-IR) spectra were recorded using a PerkinElmer Frontier instrument. X-ray diffraction (XRD) patterns were acquired at a scanning rate of 1°per minute. The chemical composition and morphology of the DFPI and NTPI COFs films were investigated using scanning electron microscopy (SEM; Carl Zeiss AG, Germany) integrated with energy-dispersive spectroscopy (EDS). The HRTEM images of DFPI and NTPI COFs films were determined using transmission electron microscopy (TEM, JEM2100F). X-ray photoelectron spectroscopy (XPS) data were collected on PHI 5000 VersaProbe III. All the electrochemical properties were measured using a CHI 760 (P. R. China) electrochemical workstation. The active area of the electrochromic film is 1.5 cm^2. Cyclic voltammetry (CV) curves of the DFPI and NTPI COFs films were acquired in a 0.1 mol/L TBAP electrolyte solution. The Pt thread, DFPI or NTPI films electrodes, and Ag/AgCl were used as the counter electrode (CE), working electrode(WE), and reference electrode (RE), respectively. In the frequency range of 1-10^6 Hz, the electrochemical AC impedance spectra (EIS) of the DFPI and NTPI COFs films were obtained. The energy-storage properties of the DFPI and NTPI COFs films were tested under constant current charge and discharge conditions. The spectroelectrochemistry and electrochromic properties of DFPI and NTPI COFs films were measured on the electrochromic cycle tester (Zhuhai Kaivo Optoelectronics Technology Co., Ltd.) integrated with an ultraviolet-visible (UV–*vis*) spectra spectrophotometer (Thermo Helios-γ UV–vis spectrometer) using a double electrode system (WE: DFPI or NTPI film electrode,_CE: Pt thread). The optical spectrum of clean ITO glass was used as the baseline. The Raman spectra were carried out at room temperature by a Raman spectrometer (i-Raman Plus, B&W TEC Inc). The Raman spectra were recorded under 785 nm laser excitation, the beam spot focused to ca. 80 mm in diameter and the excitation power is 120 mW with the spectrum acquisition time of 10 s. The potential of the working electrode is increased in small steps. After each potential increase, a waiting period is made until a quasi-

equilibrium state is reached, and then the Raman spectrum is recorded "in-situ". It was assumed that the equilibrium state was reached when the potential change induced current became negligible.

S3. Synthetic procedures of PM-TPI COF film

DFPI or NTPI COF films were prepared by constant potential deposition integrated with low-temperature annealing. Firstly, the DFPI or NTPI COF films were synthesized by electropolymerization of 0.001 mol/L TPPDA and 0.002 mol/L DFD or NTPDA under a constant voltage of +1.0 V (*vs.* Ag/AgCl) for 200 s, respectively, in 0.1 mol/L tetrabutylammonium perchlorate (TBAP) dichloromethane electrolyte on transparent indium tin oxide (ITO) electrodes. Thereafter, The crystallinity of DFPI and NTPI COF films was further improved by low-temperature (100°C) annealing process for 8 hours.

Results and discussion

Figure S1. ^{1}H NMR spectra of DFPI COF

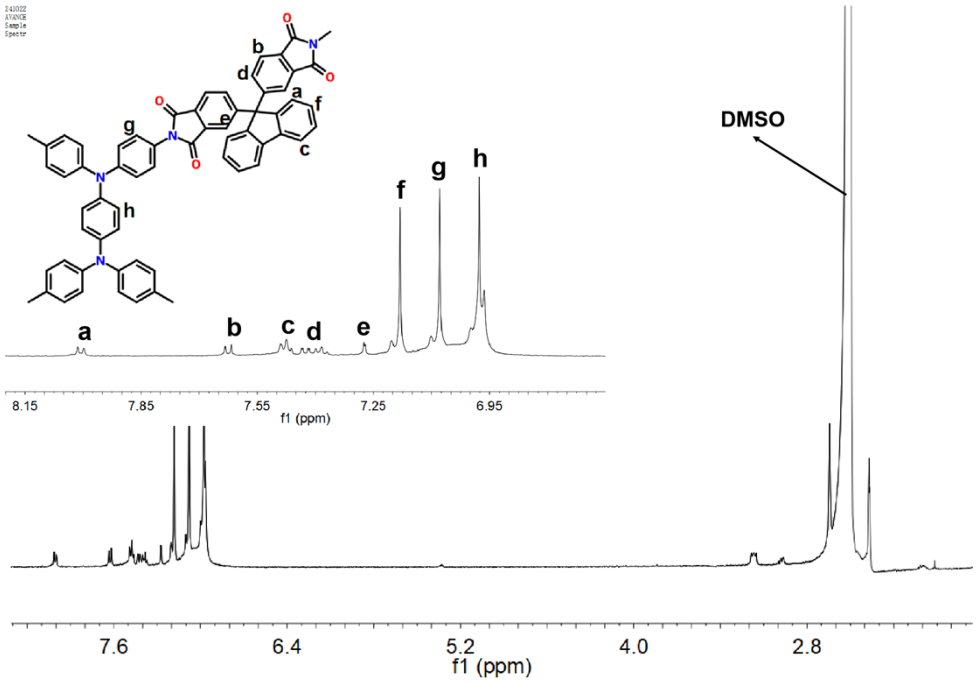

Figure S1. [1]H-NMR spectra of DFPI COF.

Figure S2. [1]H NMR spectra of NTPI COF

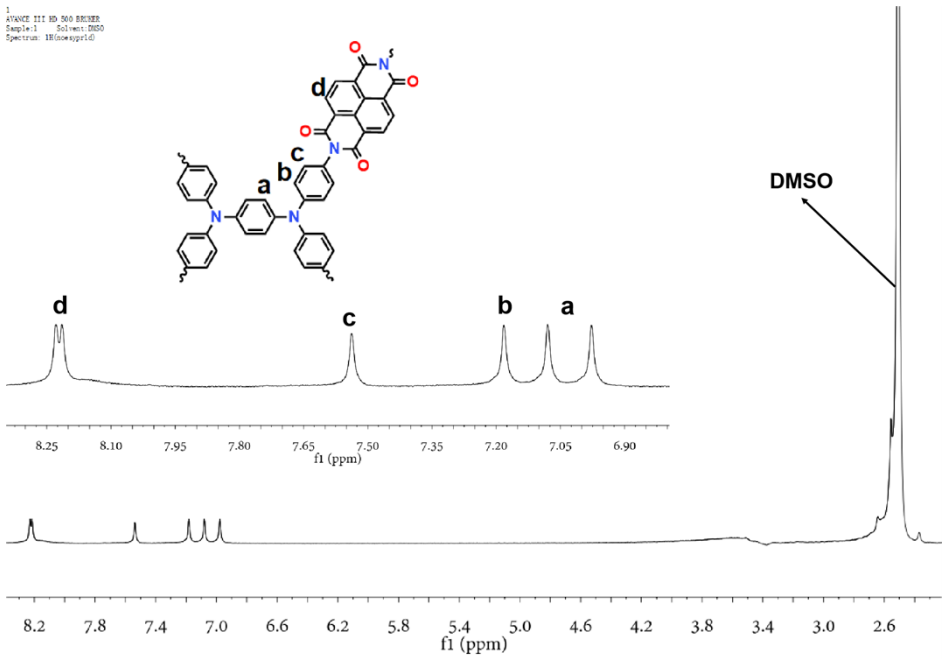

Figure S2. [1]H-NMR spectra of NTPI COF.

Figure S3. XRD patterns of TPPDA, NTCDA and DFD.

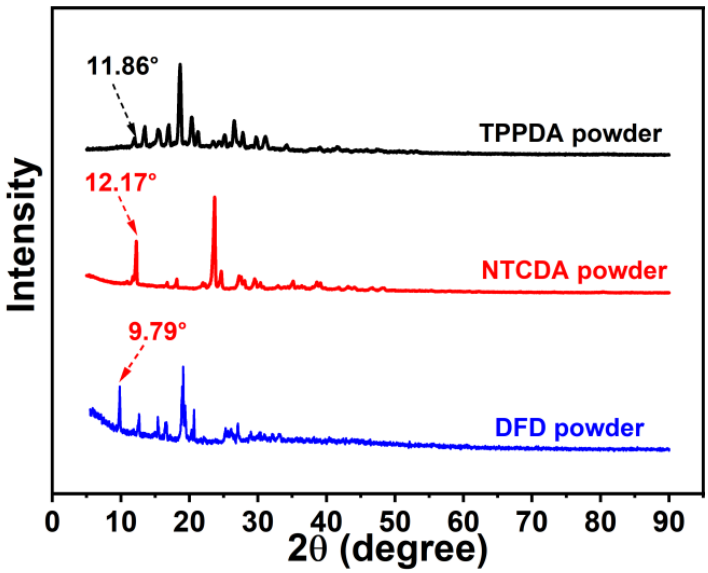

Figure S3. XRD patterns of TPPDA, NTCDA and DFD powders.

Figure S4. HRTEM images of DFPI COF film

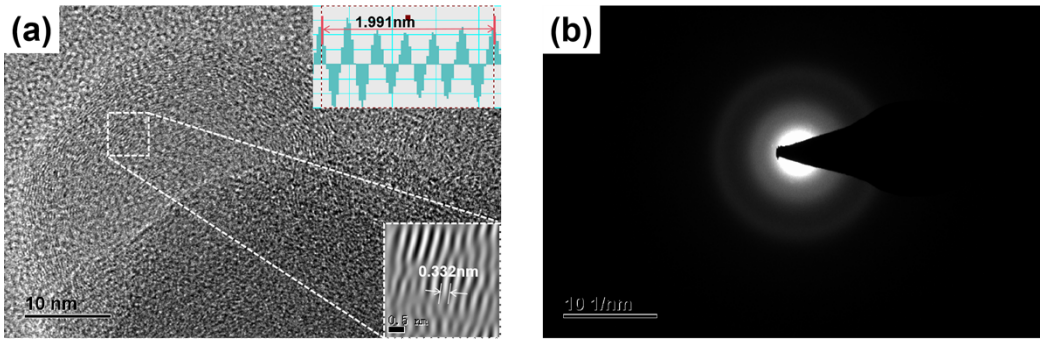

Figure S4. a) HRTEM image and b) electronic diffraction pattern of DFPI COF film.

Figure S5. N_2 adsorption and desorption curves and pore size distribution

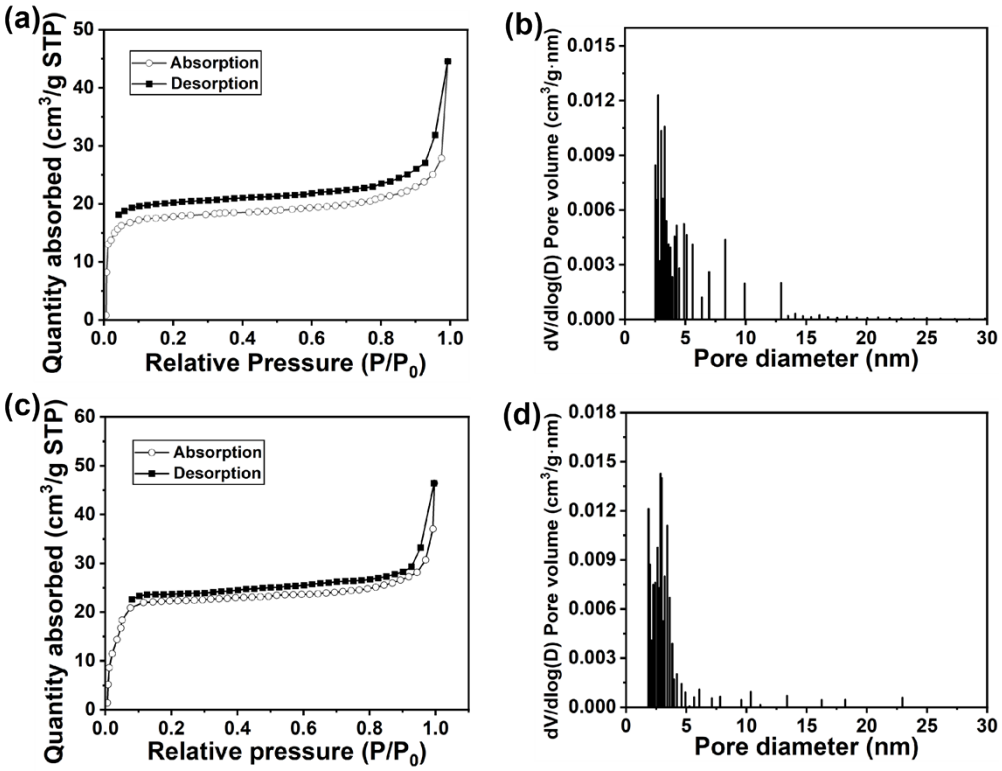

Figure S5. N_2 adsorption and desorption curves of a) DFPI COF and c) NTPI COF at 77K. Pore size distribution of b) DFPI COF and d) NTPI COF.

Figure S6. Surface morphology and EDS images of DFPI COF film without annealing

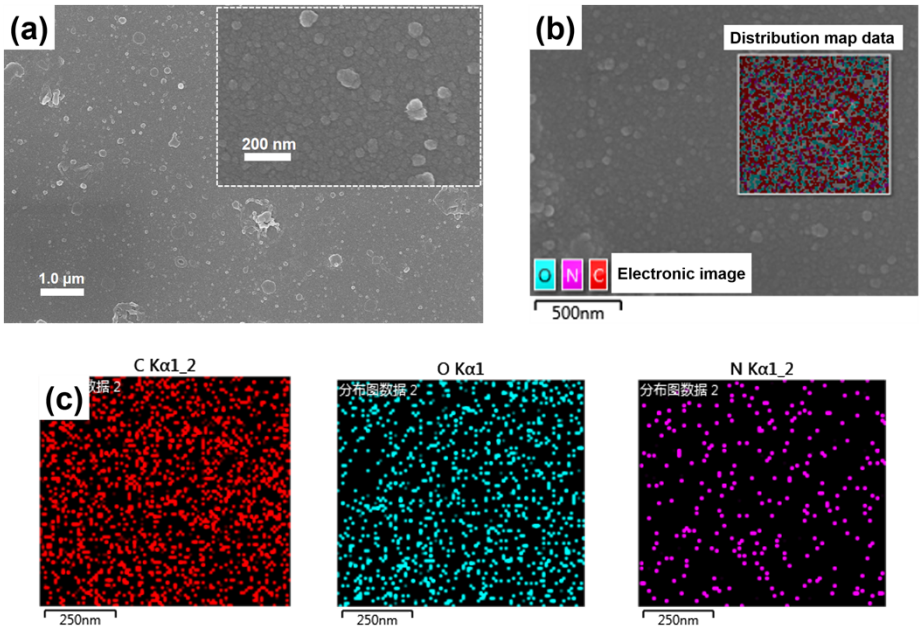

Figure S6. a) surface morphology and b), c) EDS of DFPI film.

Figure S7. Surface morphology and EDS images of NTPI COF film without annealing

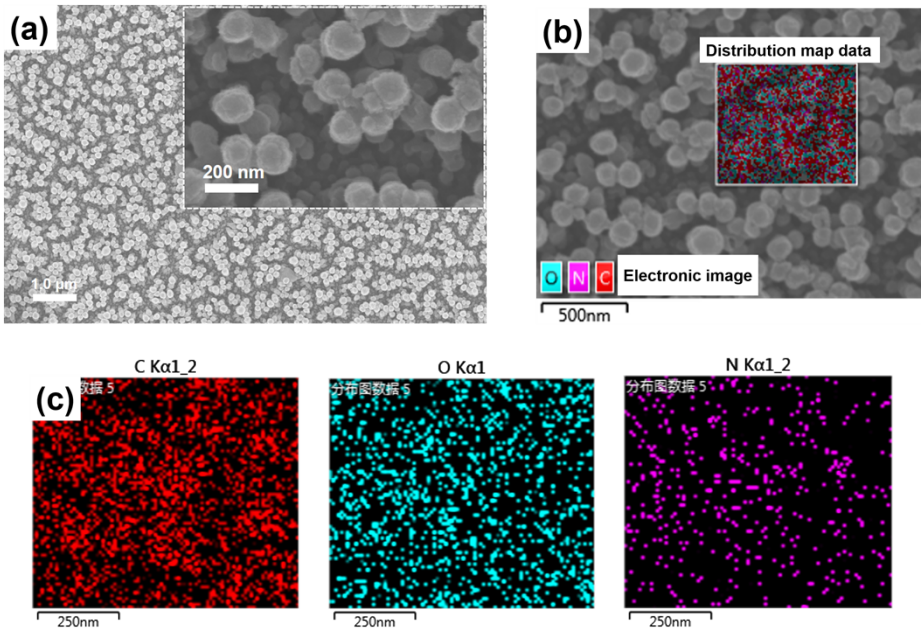

Figure S7. a) surface morphology and b), c) EDS of NTPI film.

Figure S8. AFM images of DFPI film

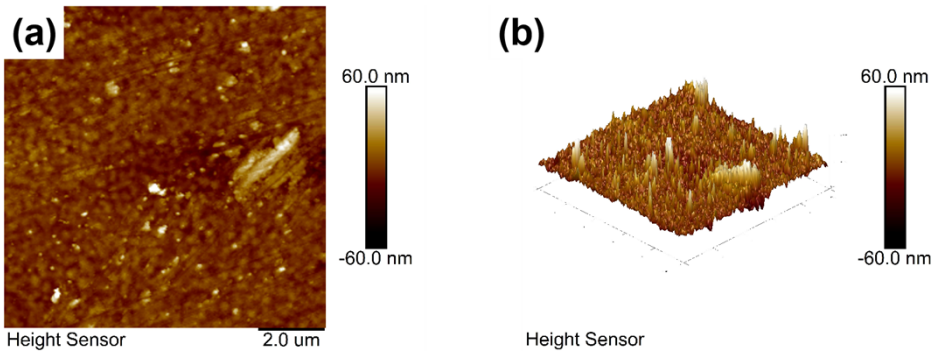

Figure S8. AFM images of DFPI COF film.

Figure S9. Thickness of DFPI COF film

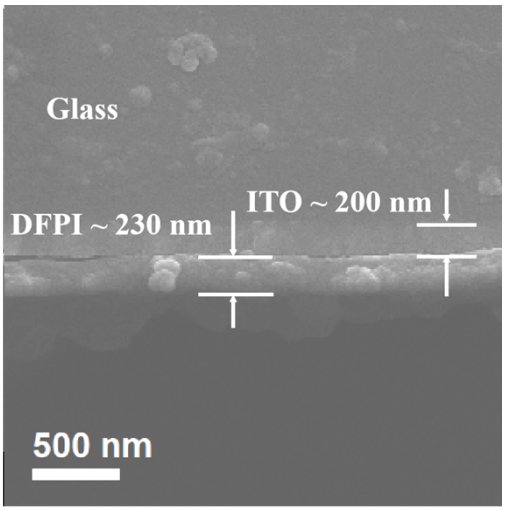

Figure S9. Sectional SEM image of DFPI COF film.

Figure S10. LSV of compounds

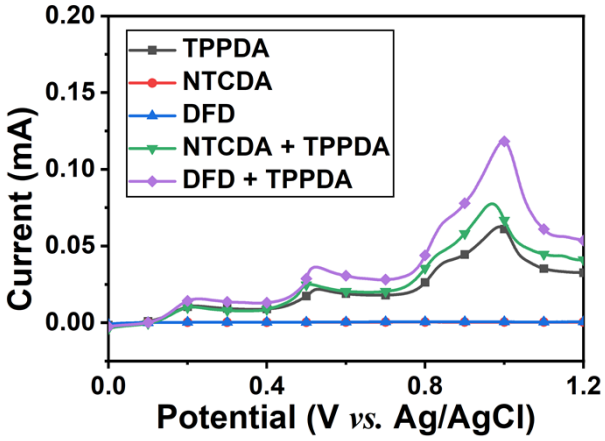

Figure S10. LSV curves of TPPDA, DFD, NTCDA compounds.

Figure S11. In-situ UV-vis spectra of compound solution at different voltages

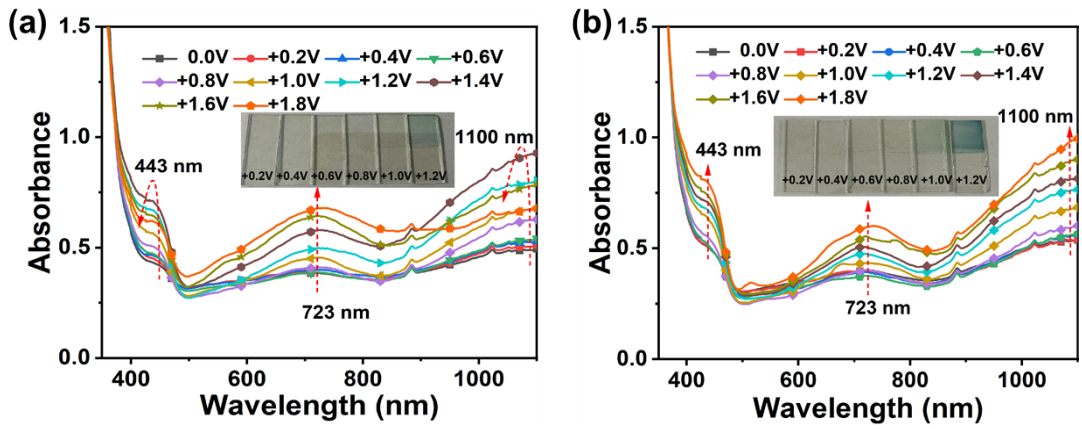

Figure S11. In-situ UV-vis spectra of a) TPPDA solution, b) TPPDA and DFD solution at different voltages.

Figure S12. In-situ Raman spectra of DFD and NTCDA solution at different voltages

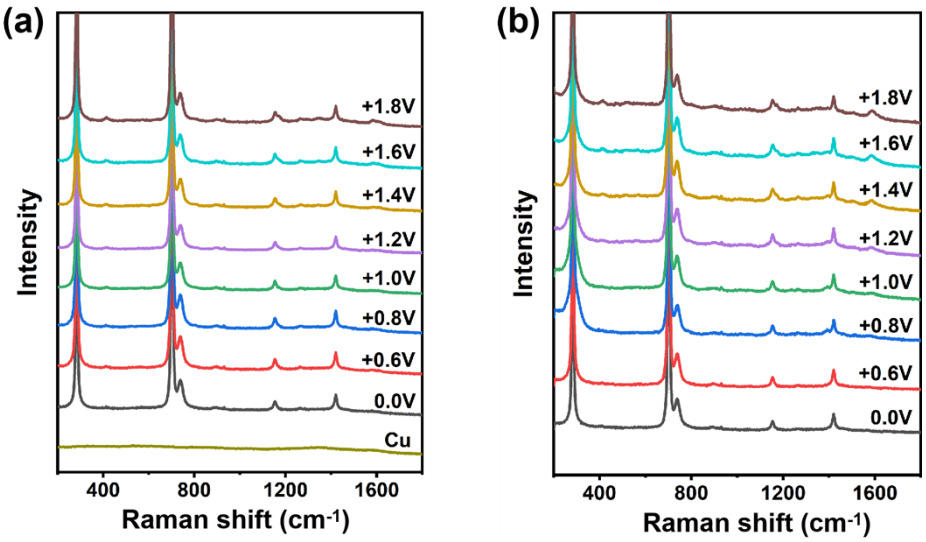

Figure S12. In-situ Raman spectra of a) DFD solution, b) NTCDA solution at different voltages.

Figure S13. In-situ Raman 2D spectra of TPPDA solution at different voltages

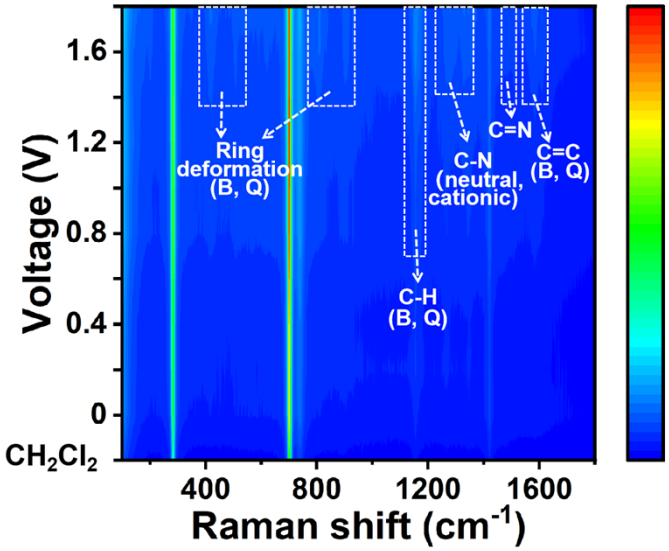

Figure S13. In-situ Raman 2D spectra of TPPDA solution at different voltages.

Figure S14. In-situ Raman spectra of TPPDA and DFD solution at different voltages

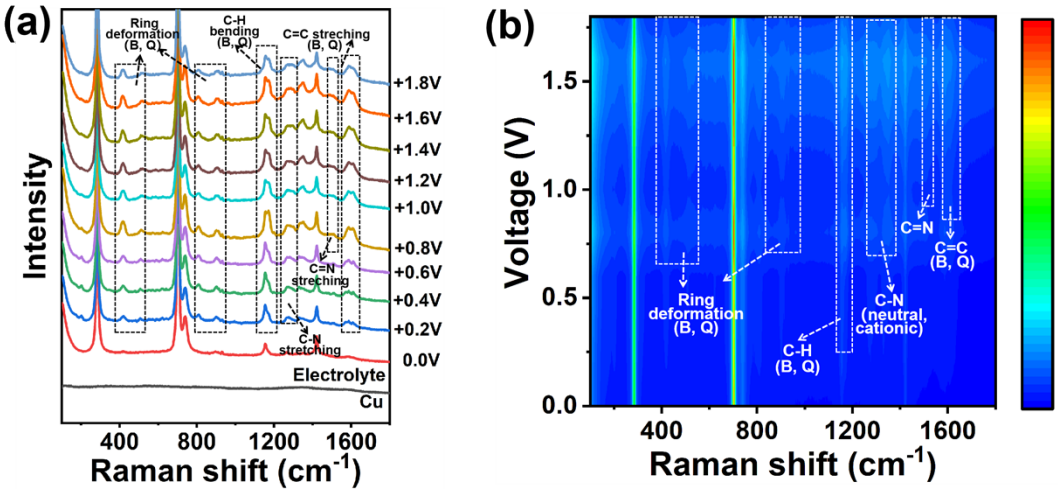

Figure S14. In-situ Raman a) 1D and b) 2D spectra of TPPDA and DFD solution at different voltages.

Figure S15. In-situ UV-vis spectra of compounds electropolymerization

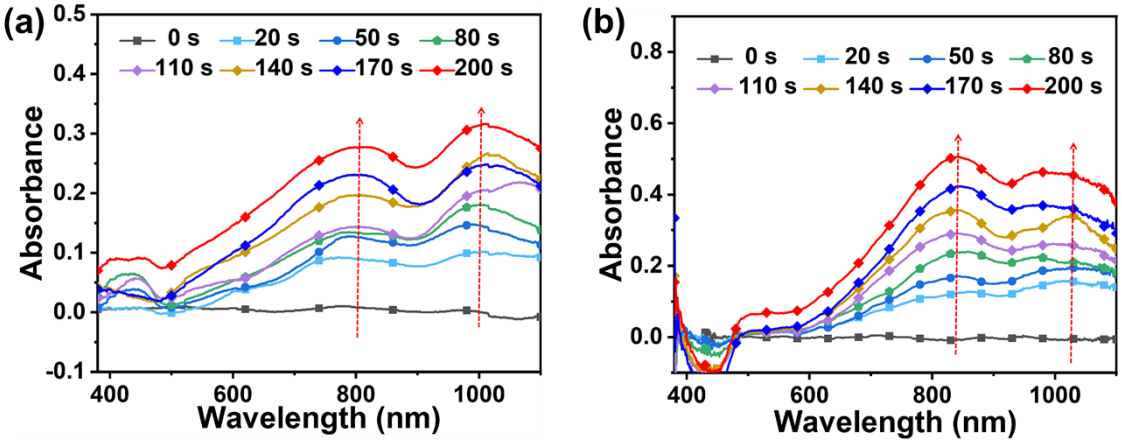

Figure S15. In-situ UV-*vis* spectra of a) TPPDA, b) TPPDA and DFD for 200 s electropolymerization at +1.0 V voltage.

Figure S16. CV curve and electrochemical redox mechanism of DFPI COF film

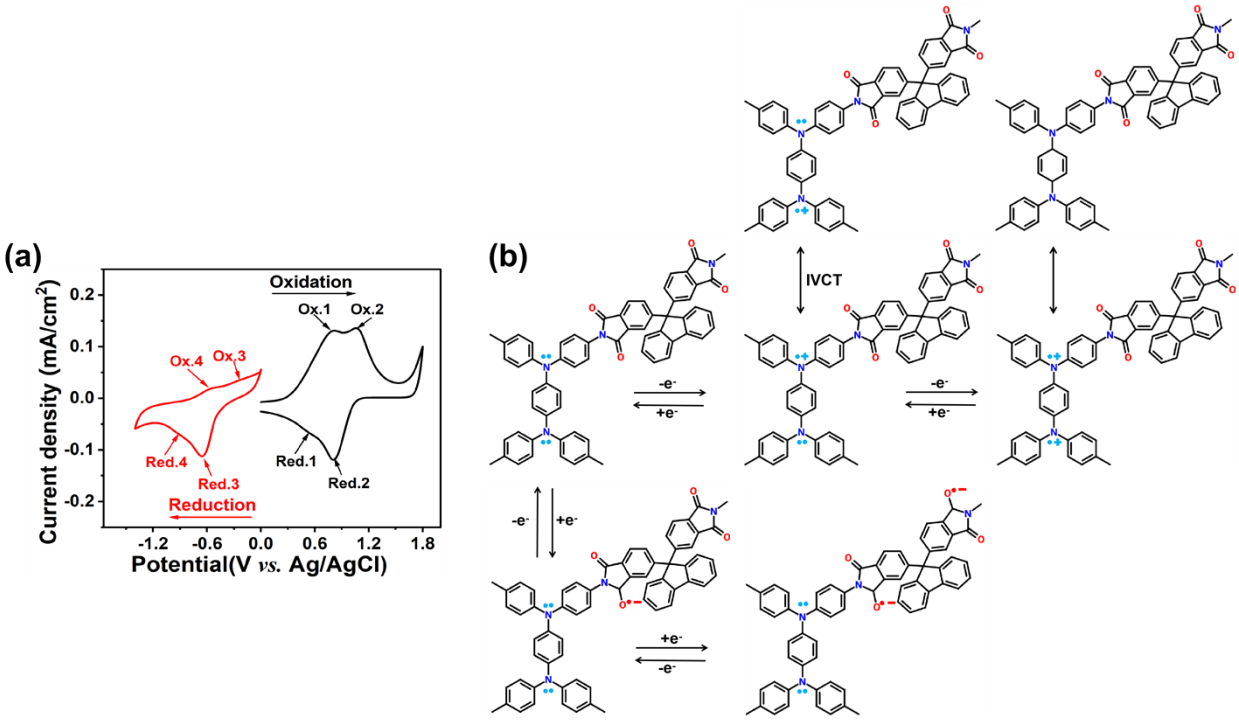

Figure S16. a) CV curves, b) mechanism of electron gain and loss during electrochemical redox process of DFPI COF film.

Figure S17. CV curve and electrochemical redox mechanism of NTPI COF film

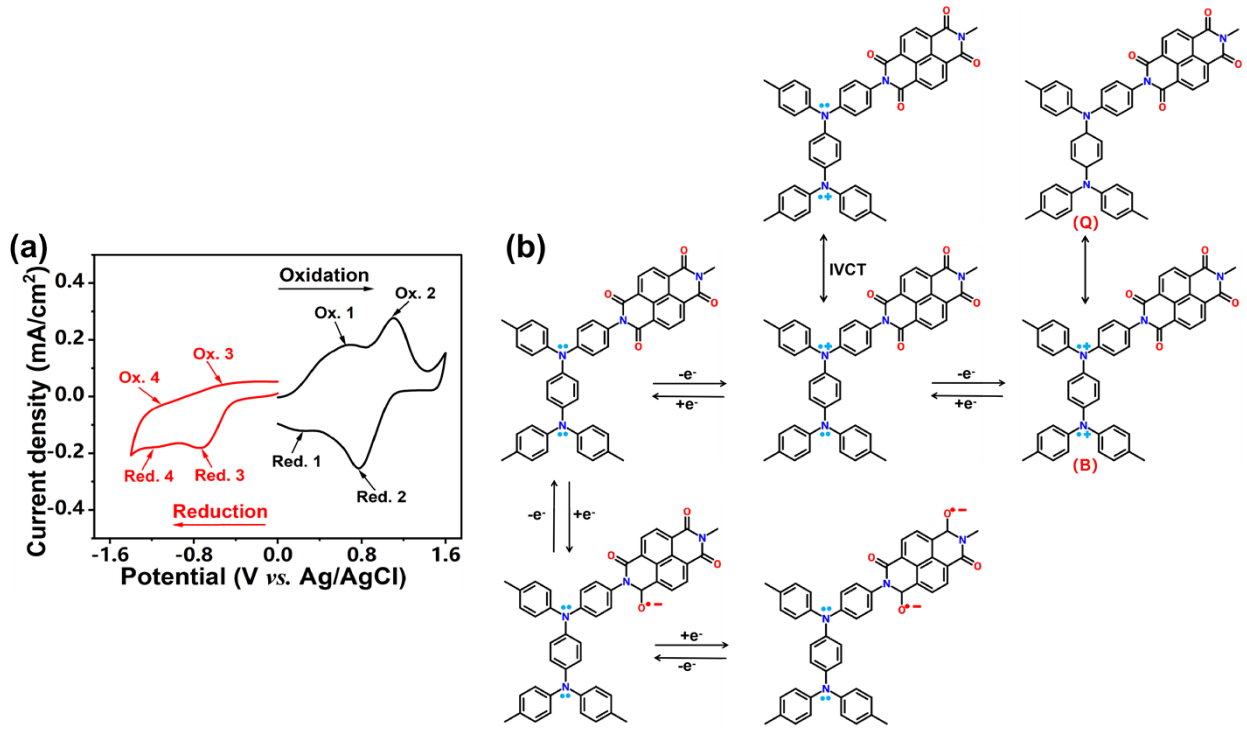

Figure S17. a) CV curves, b) mechanism of electron gain and loss during electrochemical redox process of NTPI COF film.

Figure S18. CV curves of DFPI COF film at different scan rates

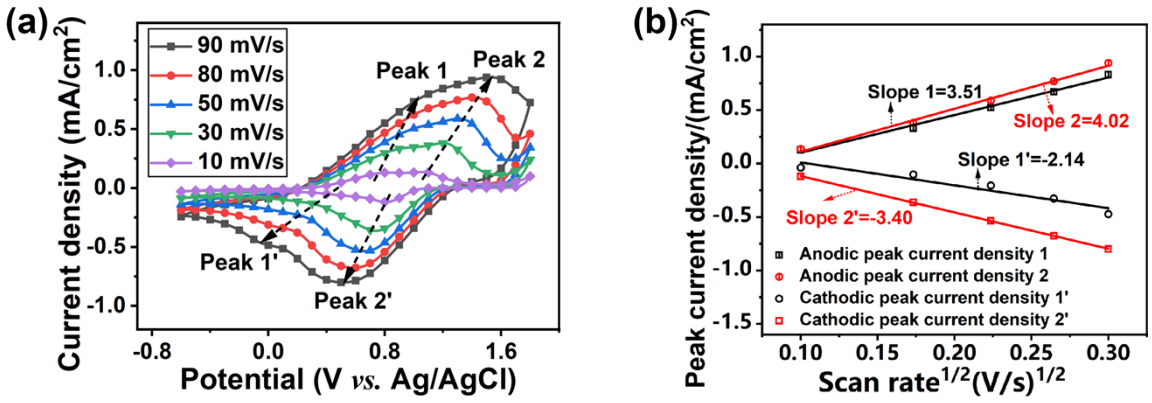

Figure S18. a) CV curves at different scan rates (v), b) plots of peak current density (i_p) *vs.* v of DFPI COF film.

Figure S19. Nyquist plots of DFPI and NTPI COF films

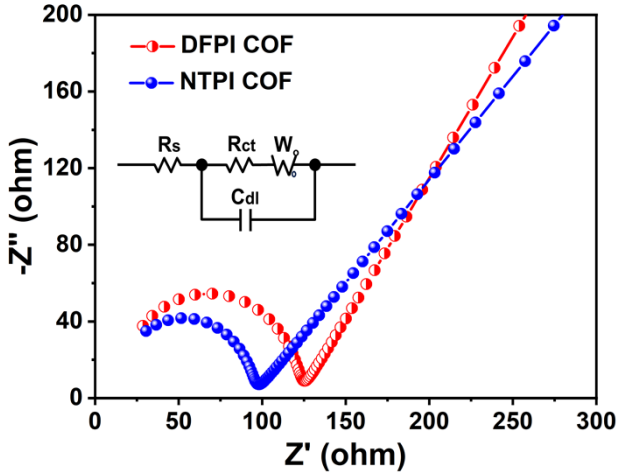

Figure S19. EIS of DFPI and NTPI COF film electrodes.

Figure S20. Spectroelectrochemistry of DFPI COF film

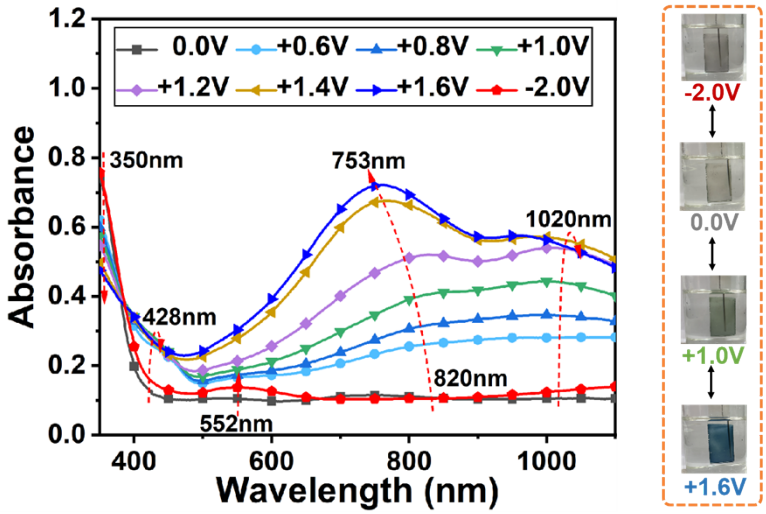

Figure S20. Spectroelectrochemistry of DFPI COF film.

Figure S21. In-situ Raman spectra of DFPI COF film during electrochromic process

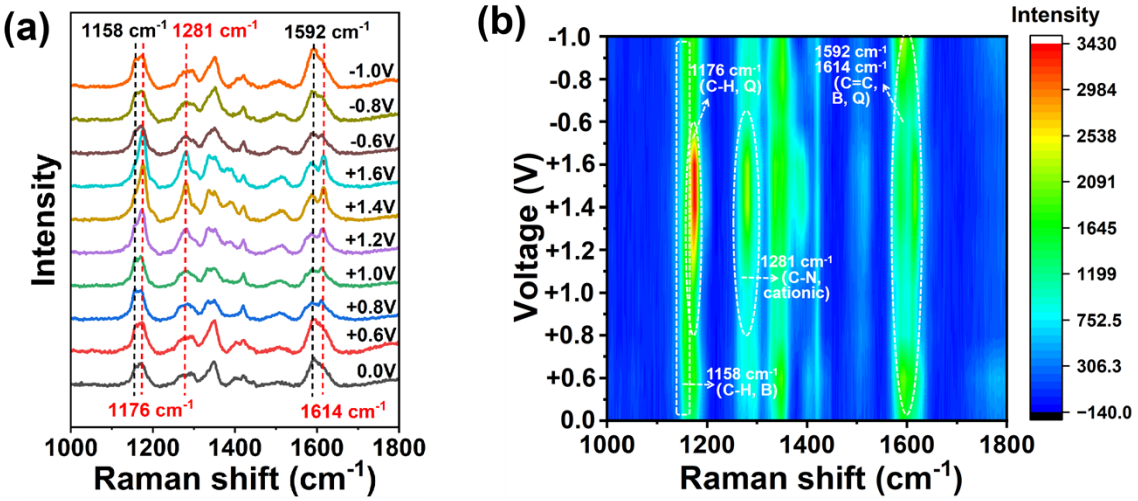

Figure S21. a) 1D and 2D spectra of DFPI COF film during electrochromic process.

Figure S22. XPS spectra of DFPI COF film under bleached and anodic colored states

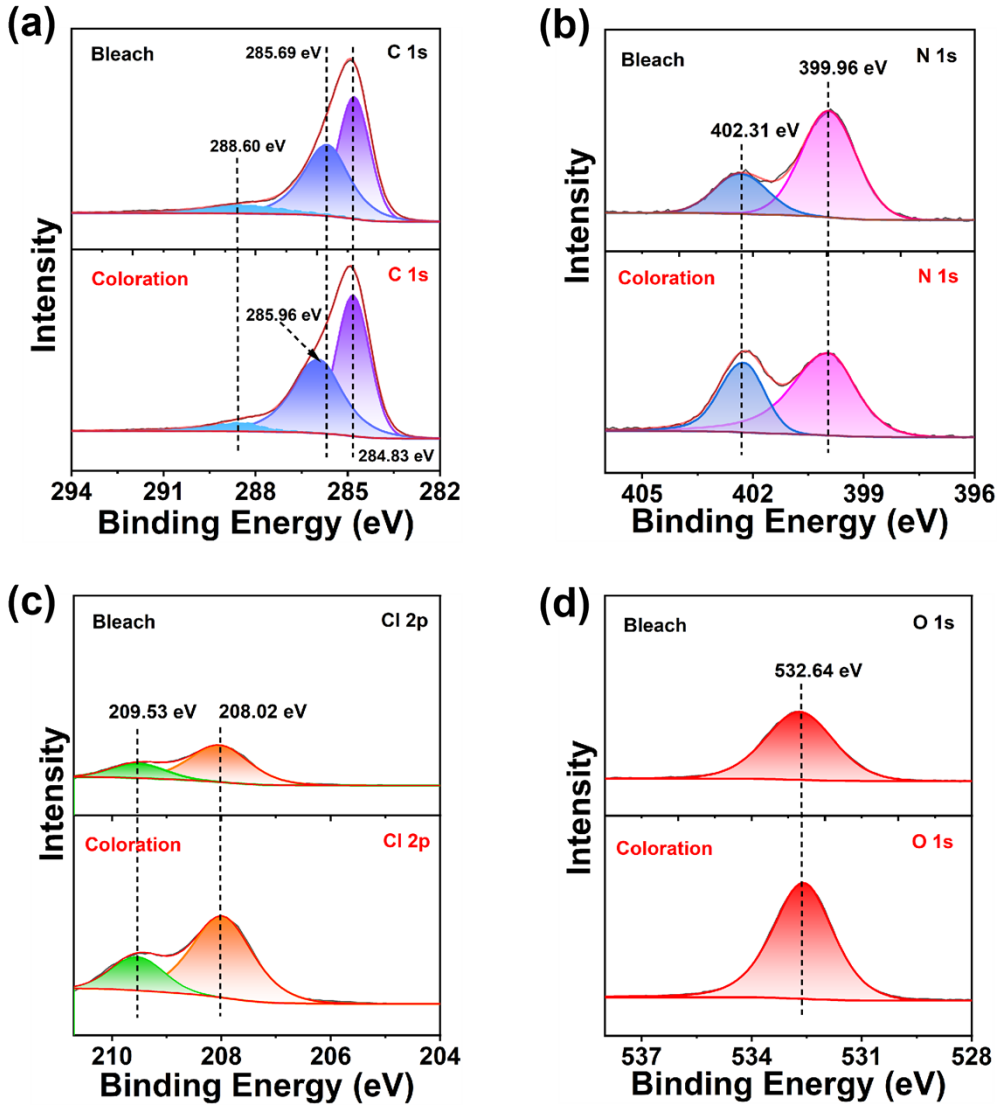

Figure S22. XPS a) C 1s, b) N 1s, c) Cl 2p, and O 1s spectra of DFPI COF film at bleached and anodic colored states.

Figure S23. XPS O 1s spectra of NTPI COF film under bleached and anodic colored states

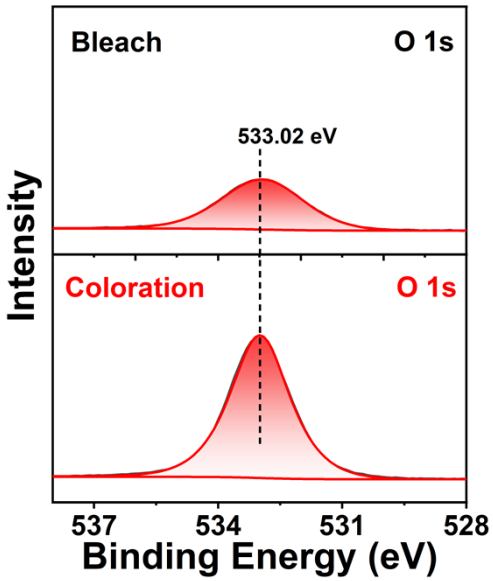

Figure S23. XPS O 1s spectra of NTPI COF film at bleached and anodic colored states.

Figure S24. XPS spectra of DFPI COF film under cathodic colored states

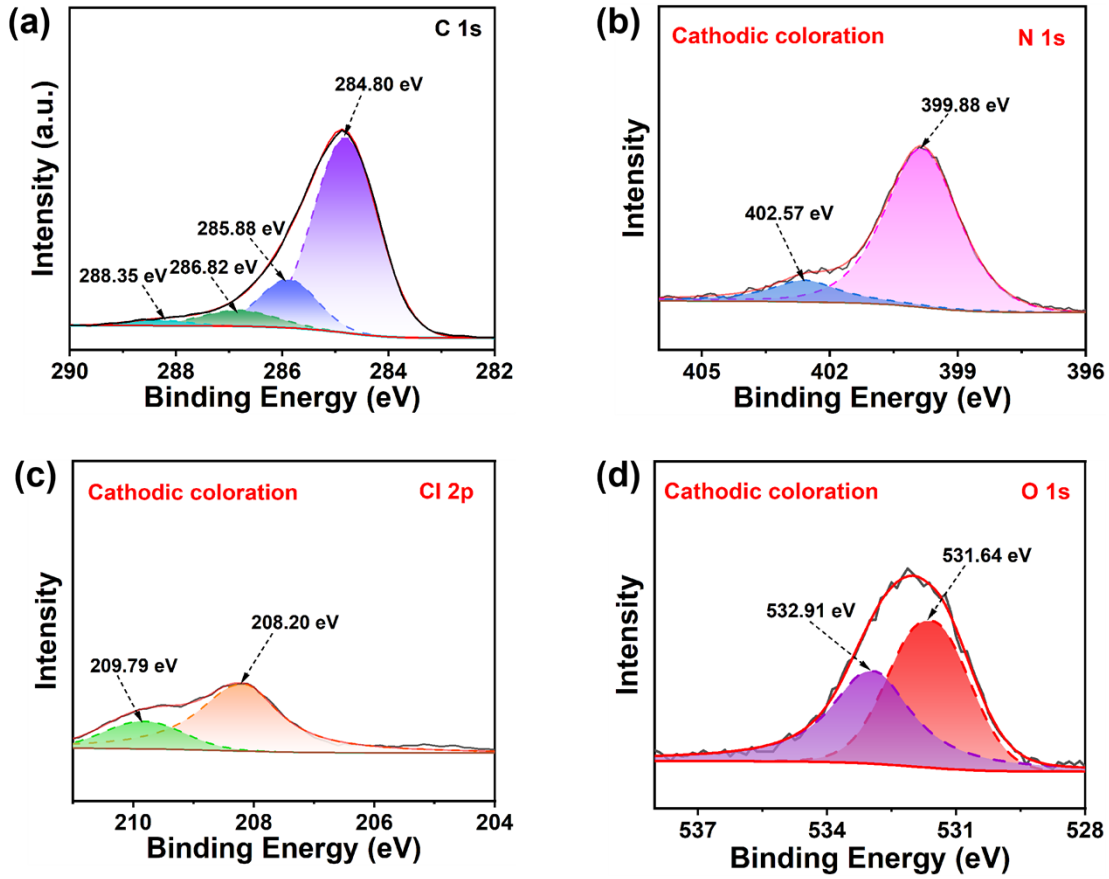

Figure S24. XPS a) C 1s, b) N 1s, c) Cl 2p, and O 1s spectra of DFPI COF film at cathodic colored states.

Figure S25. XPS spectra of NTPI COF film under cathodic colored states

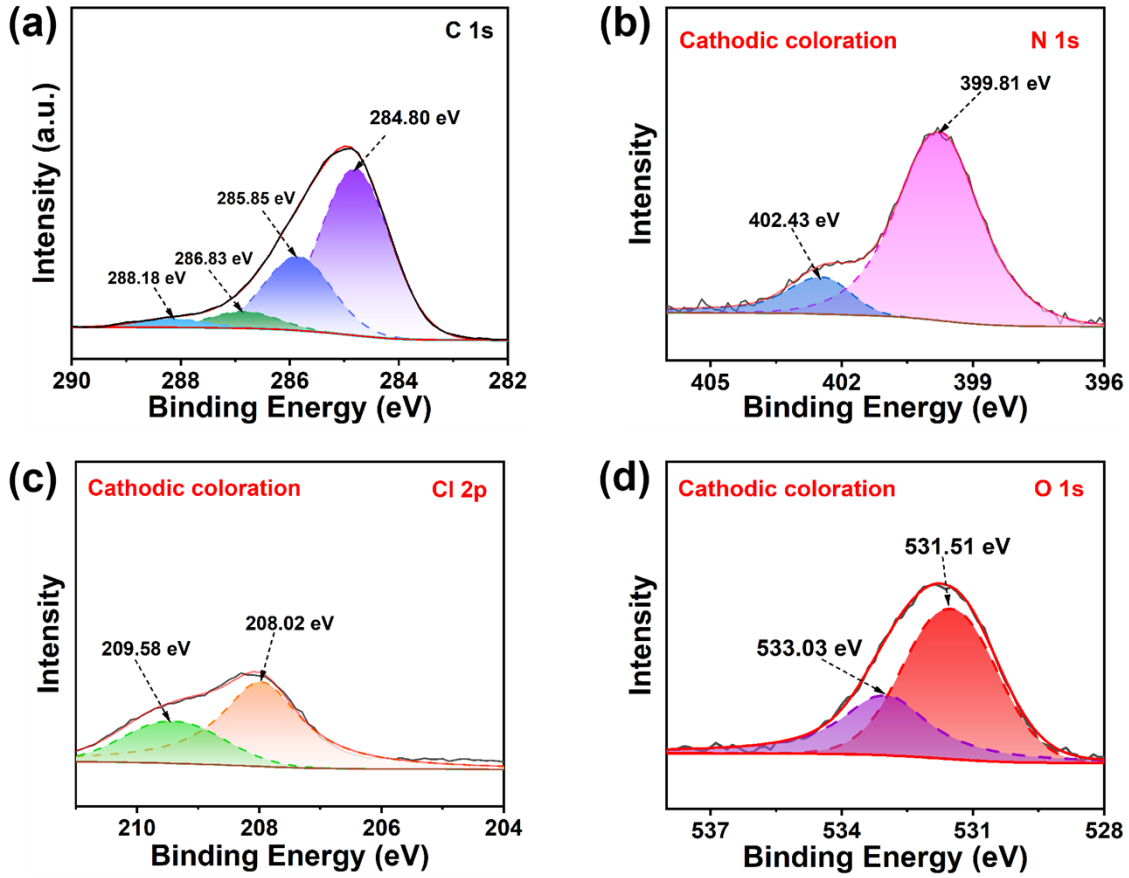

Figure S25. XPS a) C 1s, b) N 1s, c) Cl 2p, and O 1s spectra of NTPI COF film at cathodic colored states.

Figure S26. Cycling life of DFPI COF film

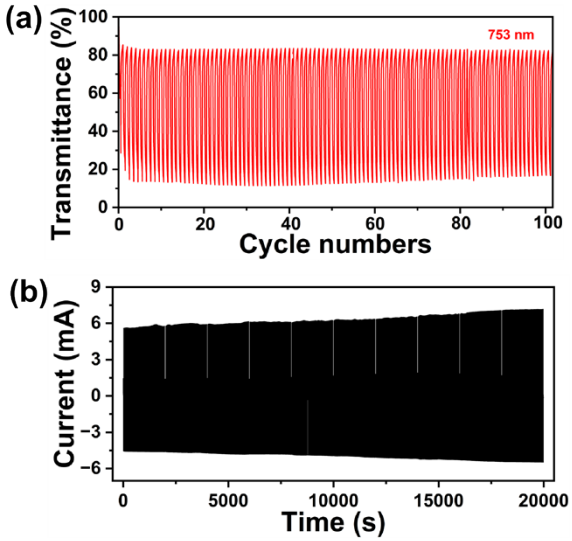

Figure S26. a) Curves of transmittance vs. cycle numbers of DFPI COF film at 810 nm under square wave voltages, b) the curves of current *vs.* time of DFPI COF film during 1000 cycles.

Figure S27. Raman spectra of long-term cycles

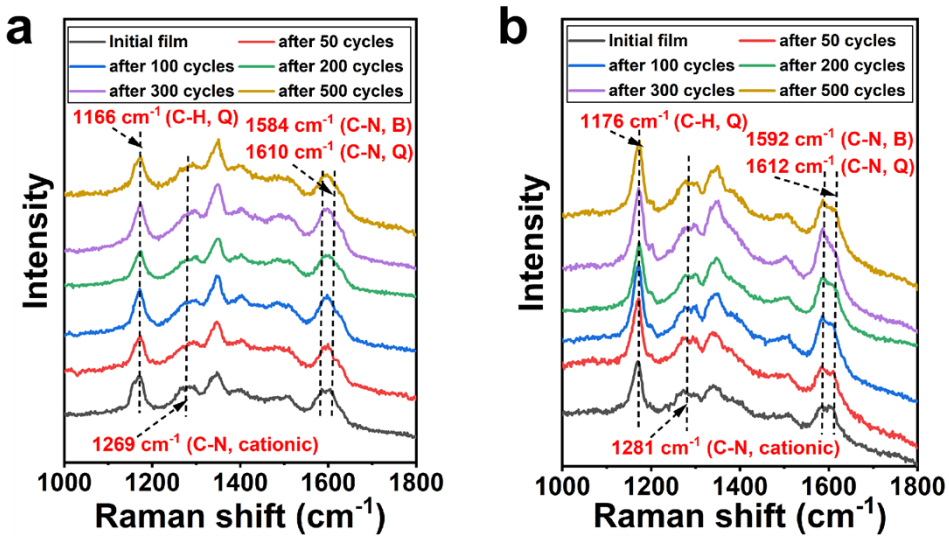

Figure S27. Raman spectra of a) DFPI COF and b) NTPI COF films after 50, 100, 200, 300, and 500 cycles.

Figure S28. FT-IR spectra of DFPI COF and NTPI COF films after 1000 cycles

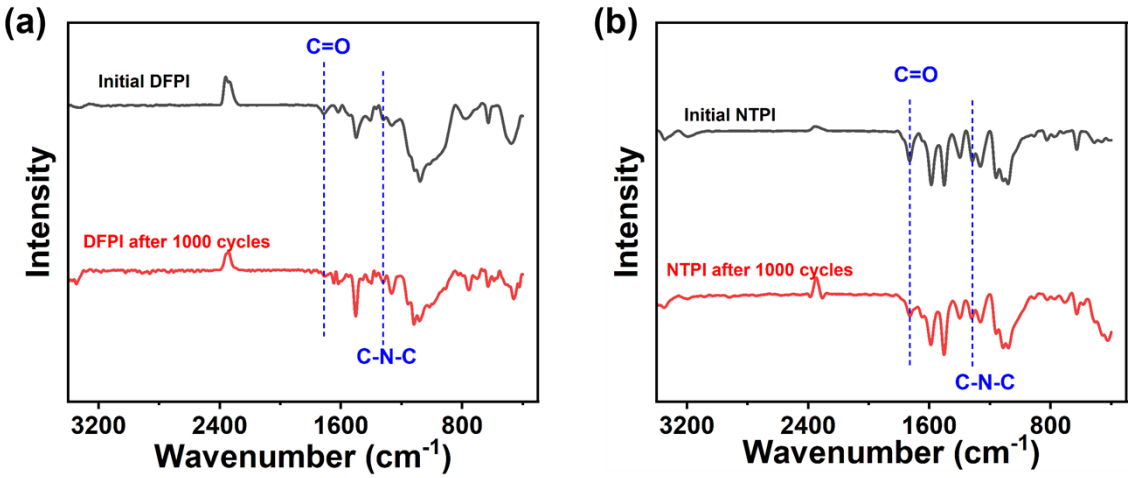

Figure S28. FT-IR spectra of a) DFPI COF and b) NTPI COF films after 1000 cycles.

Figure S29. Coloration efficiency of DFPI and NTPI COF films

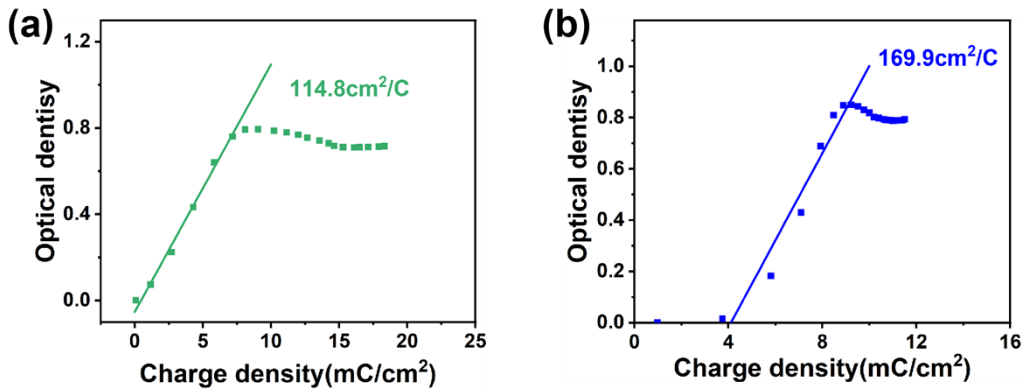

Figure S29. Coloration efficiency of a) DFPI and b) NTPI COF films.

Figure S30. Spectroelectrochemistry of DFPI COF-based flexible ECD

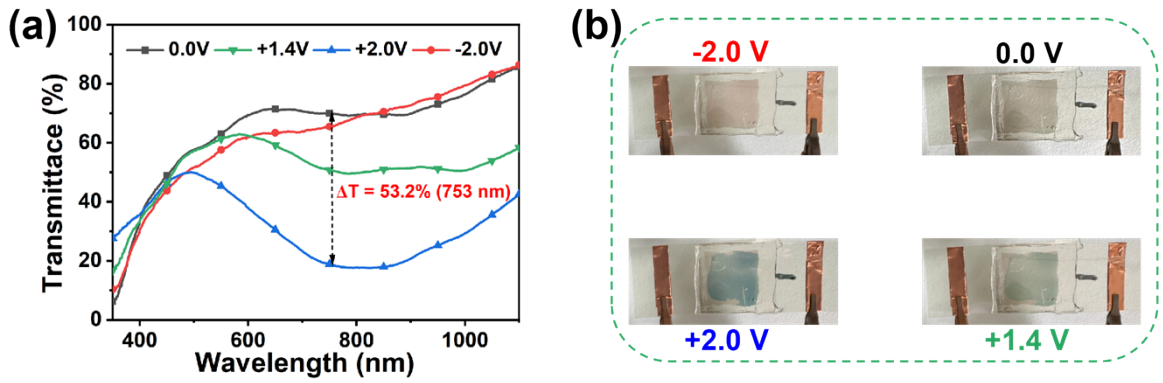

Figure S30. a) Optical transmittance and b) digital photos of DFPI COF film at bleached/colored states.

Table S1. D_{ClO4^-} and R_{ct} of DFPI and NTPI COFs film electrodes

Table S1. D_{ClO4^-} and R_{ct} of DFPI and NTPI COFs film electrodes

D_{ClO4^-} (cm^2/s)	DFPI	NTPI
$D1_{ClO4^-}$ (insertion) (cm^2/s)	7.57×10^{-9}	2.47×10^{-8}
$D1_{ClO4^-}$ (extraction) (cm^2/s)	2.81×10^{-9}	1.84×10^{-8}
$D2_{ClO4^-}$ (insertion) (cm^2/s)	1.24×10^{-9}	1.98×10^{-9}
$D2_{ClO4^-}$ (extraction) (cm^2/s)	8.87×10^{-10}	2.78×10^{-9}
R_{ct} (Ω)	108.7	82.67